ISSN: 0974-5823 Vol. 7 No. 2 February, 2022

International Journal of Mechanical Engineering

Reverse Osmosis (RO) Coupled by PV Solar Energy For the Demineralization of Borehole Water (BW) in The Ain El Atti Region

A. Maftouh*

LPHE-Modeling & Simulations, Faculty of Science, Mohammed V University in Rabat, Rabat, Morocco.

O. El Fatni

LPHE-Modeling & Simulations, Faculty of Science, Mohammed V University in Rabat, Rabat, Morocco

T. Bahaj

Geosciences, Water and Environment Laboratory, Faculty of Science, Mohammed V University in Rabat, Rabat, Morocco

I. Kacimi

Geosciences, Water and Environment Laboratory, Faculty of Science, Mohammed V University in Rabat, Rabat, Morocco

S. El Hajjaji

Laboratory of Spectroscopy, Molecular Modeling, Materials, Nanomaterials, Water and Environment, (LS3MN2E-CERNE2D), Chemistry Department, Faculty of Sciences, Mohammed V University in Rabat, Rabat, Morocco

Abstract - Our work comprises of a sizing study of Ain El Atti Borehole Water Reverse Osmosis (BWRO) demineralization plant coupled with photovoltaic (PV) solar for the supply of fresh water in the Ain El Atti region in the province of Errachidia. The main goal of this research was to model and simulate demineralization of borehole water by RO powered with PV solar energy. Two different tools were used in this regard, the first one is Integrated Membrane Solutions Design (IMSDesign) software for the simulation of performance and energy estimation of Ain El Atti Borehole Water RO system. The second one is PVsyst software to model the performance of a small-scale photovoltaic (PV) solar system using four different PV system scenarios, which combine two different modules technologies and two different solar inverters to obtain the best possible scenario in the Ain El Atti area. Results showed that employing the Hydranautics advanced membranes can enable us to produce freshwater with lower energy consumption. Concerning the PV system, the calculation methodology by using PVsyst is divided into further design calculations, energy calculations, and evaluation parameter calculations. The number of PV modules in the system, the number of PV modules in series and parallel, and the total installed capacity are the calculation parameters. Evaluation parameters such as performance ratio (PR) are also calculated. As a result, the scenario with the greatest outcomes is the one that employs thin-film CdTe module technology and the highest nominal power inverters. Consequently, if demineralization of borehole water remains the ultimate solution for freshwater feed, the choice of coupling with PV offers a promising prospect for covering the electricity and water needs in the Ain El Atti region.

Keywords: *Demineralization; Reverse Osmosis (RO); Solar energy (PV); ROPV coupling; IMSDesign-2015; Ain El Atti.*

INTRODUCTION

Hydraulic resources scarcity is the most serious worldwide problem for humanity, in both quantitative and qualitative aspects. The sub-desert region of Tafilalet bears witness to this phenomenon, which hinders its socio-economic development [1]. Indeed, the succession of years of drought has contributed enormously to the reduction of arable land and has led to massive waves of migration of inhabitants [2]. However, the construction of the Hassan Addakhil dam made it possible to reduce the climatic hazards along the course of the Wadi Ziz where the largest palmeraie of Morocco could survive besides a narrow strip of intensely exploited land along this course of water [3]. However, the volumes of water that can be mobilized remain insufficient to meet the needs of a region experiencing very strong economic and social growth [4].

The catchment field of Ain El Atti consists of many artesian boreholes that were made in the 1980s. The Infra-Cenomanian aquifer extends longitudinally between the centre of Tinghir in the west and the centre of Bouannane in the east, and laterally between the mountain ranges of High Atlas in the north and those of the Anti-Atlas in the south. It is mainly consisting of detrital rocks (sand, sand-stone and clay) with a thickness ranging from a few tens of meters to 250 m in its flush part and a few hundred meters undercover. The capture field of Ain El Atti provides an average flow of 18 l/s. These boreholes capture the aquifer, which in principle was intended to ensure the drinking water supply of the surrounding inhabitants. However, the aquifer exploited this way is very rich in brines. This aquifer is fed by linkages with the tablecloths of the High Atlas, by infiltrations of rain and floodwater and releases Hassan Addakhil dam. The water level of the water table is between 5 and 90 m underground surface, and the piezometric level ranges from 5 to 75 m in the sub-recovery part, whereas the aquifer is locally artesian between Douira and

Erfoud (see in Fig.1). The Infra-Cenomanian aquifer has a transmissivity of between 2.2 x 10^{-4} and 2 x 10^{-2} [5]. The increased pressure on water resources and its impact raises concerns about the exploitation of existing groundwater. Indeed, a large part of its resources is not exploitable due to their poor quality (high salinity) and because of the high depth. In this case, the infra-Cenomanomanic tablecloth of Ain El Atti is addressed [6].

Reverse Osmosis (RO) membrane is a barrier technique used to produce potable water from both seawater (SW) and brackish water (BW) desalination [7–9]. Moreover, the market for RO membranes has expanded fast. The low power consumption of the RO system, which is 2–3 kWh/m^3 [10–12], is one of its key benefits. To meet the expanding water demand, however, the inventive development of RO technology to deliver more energy savings is continually required. Desalted water generated in large-scale desalination facilities now costs between 0.5 and 1.20 \$/m^3 [13,14]. As a result, in recent decades, several researchers have devised various innovative RO desalination topologies that use multiple membrane stages and recycling streams to simultaneously lower specific energy consumption (SEC) and boost water recovery [15–18]. This is accomplished by adjusting the process parameters [19–20], even explaining the separation strategy and doing model-based optimization to increase the efficiency of the manufacturing process [21–23]. Feed pretreatment and brine management costs will fall as water recovery increases [24], boosting the process's economics significantly. Since the 1990s, however, RO desalination facilities have required less energy, investment and maintenance than conventional desalination procedures [25]. Today, the photovoltaic (PV) renewable energy industry exhibits a better option for solving the environmental and the exhaustion of translational energy problems [26]. PV energy coupled with Brackish Water Reverse Osmosis (BWRO) desalination offers a highly economic option in sunny locations like Ain El Atti region (south-east of Morocco) with huge potential solar energy, receiving around 2530.92 per year [27]. This bodes well for the construction of PV stations for pumping and home illumination, as well as their improvements as a result of the PV systems that are now in the news [26]. PVRO coupling is a viable option for small communities since it is easier to adopt in distant regions and is more sustainable and environmentally beneficial [28,29]. Furthermore, it is simple to build and assemble for diverse demand profiles utilizing modular components, and it is simple to maintain and repair [30]. However, in order to be a viable water solution for small towns and distant places, PVRO must be economical, which presents several challenges, such as high costs and the intermittent nature of renewable sources [31–33]. Because of differences in solar resources and water types, the overall life-cycle cost of PVRO installations varies greatly by region. According to Mohsen and Al-jayyousi [34], RO technology is highly suited for Jordan and other dry places across the world because to its appropriateness for both marine and brackish water. Furthermore, RO plants are particularly adaptable in terms of water quantity and quality, and they might be well suited to a renewable energy supply [35]. Solar energy supply can be cost-effective in many circumstances in nations with no fossil fuel resources or in rural places as compared to tiny fossil fuel desalination facilities, which are generally expensive to run in remote areas [36]. As a result, the tiny units might use solar energy to reduce their reliance on expensive fossil fuels [37]. This resource is dispersed more equally throughout the region than other renewable energy (RE) resources, which are often site-specific [38]. There are large places where this resource may be utilized [39]. The majority of existing renewable-powered desalination facilities (60 percent) use RO technology [40, 41]. Solar photovoltaic (PV) energy is the most common renewable energy source for water desalination, accounting for 43 percent of all current RE desalination facilities, followed by solar thermal and wind energy [42].

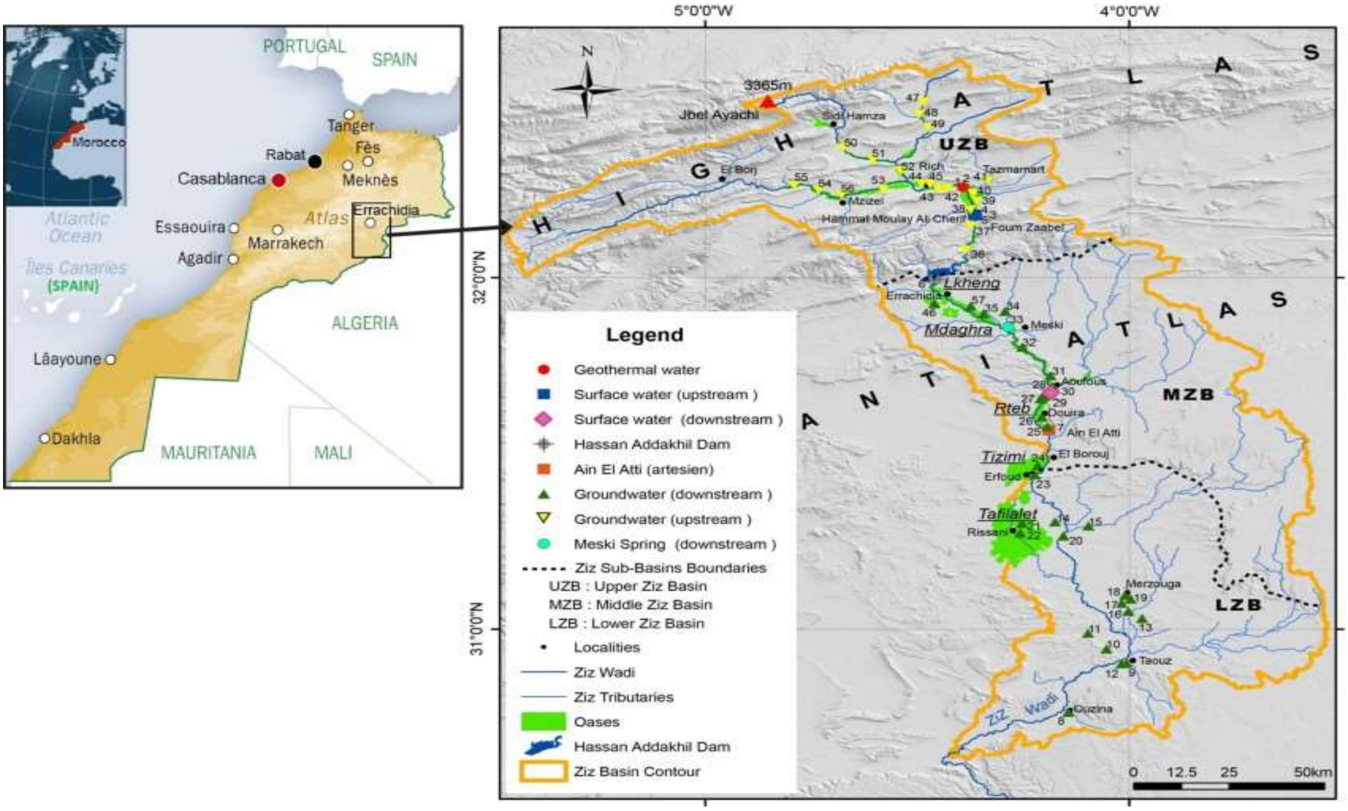

Figure 1: Study region location map displaying the geographical distribution of sampled water within the Ziz Basin [43].

The cost of electricity generation from renewable energy (0.05-0.09 $/kWh for solar-powered) against fossil fuel (0.05–0.09 $/kWh) further supports the usage of renewable energy over fossil fuel [44]. Renewable desalination has the potential to assist in meeting the issues of conventional desalination. It is predicted to become economically viable as the costs of renewable technologies continue to fall and fossil fuel prices rise [45]. The fundamental problem of integrating solar PV systems with RO desalination is that solar resources change throughout the day and night, as does the electrical energy supplied [46]. Batteries are commonly used in RO desalination plants oriented by PV to smooth electrical current and maintain steady water pressure and flow. The usage of batteries, on the other hand, dramatically raises investment and maintenance expenses. [47]. As a result, several research efforts are being conducted to store energy in the form of product water. As a result, the system may need to be somewhat enlarged to account for fluctuations in the energy sources. This can lead to lower lifespan costs and a more resilient system design that allows for standalone operation [48].

The high salinity of the waters in this artesian area is a limitation and a limit to the supply of potable water and irrigation expansion. As a result, the present research tries to maximize and use the region's water resources. In this regard, the advancement of groundwater desalination technology (RO method) in conjunction with renewable energy (PV solar) is a good and promising solution for the long-term growth of the palm grove. This article's outline is as follows:

The methods utilized for modeling and simulation of the borehole water demineralization system using RO coupled with solar photovoltaic (PV) energy are detailed in section 2. In section 3, the size of a Borehole Water Reverse Osmosis (BWRO) demineralization plant coupled with a photovoltaic (PV) solar system is calculated in detail. In this paper, the final section 4 is devoted to a brief conclusion.

METHOD OF CALCULATIONS:

The only natural water resources considered in the Ain El Atti study area are groundwaters. The main objective of this research part was the modelling and simulation of the demineralization of borehole water by RO coupled with solar photovoltaic (PV) energy in Ain El Atti.

The following tools were utilized to fulfill the study's objectives:

- Integrated Membrane Solutions (IMS) Design software [49] is a sophisticated reverse osmosis (RO) design application that estimates performance depending on membrane type. It was utilized to assess which type of membrane would result in the best design configuration for an Ain El Atti borehole water RO machine. IMSDesign is a sophisticated piece of software that allows users to create a membrane system employing Hydranautics membranes [49]. It monitors the functioning of the RO system and is specifically developed to be a user-friendly interface for RO system operators. The standardization effort adheres to ASTM standard D 4516-85, Standard Practice for Standardizing Reverse Osmosis Performance Data [50], to achieve the highest levels of data integrity.

- Several simulation software's exist and allow estimating the production of a PV installation. We, therefore, chose to work with the PVsyst software, for our simulations because this software makes it possible to create databases by introducing the irradiations at the horizontal level obtained from the PVGis software [51] by optimizing the inclination and the orientation as well than the average monthly temperatures calculated using the Wunderground website. The PVsyst simulation tool [52] is software for evaluating, sizing, and analyzing data from whole PV solar systems. This program can simulate and study networked systems, stand-alone systems, and pumping systems. PV system modeling in PVsyst was used in this work to predict the power generation of a small-scale solar PV grid-connected energy system. In this regard, four distinct PV system scenarios are used, which mix two different module technologies and two different solar inverters to get the best feasible configuration in this researched location (Ain El Atti). As a result, the energy output of all of these scenarios is utilized to estimate performance indicators such as the performance ratio, specific yield, and so on.

-

RESULTS AND DISCUSSION:

3.1 Reverse Osmosis (RO) unit design parameters:

3.1.1 Water quality at the RO inlet:

The salinity of the raw water determines its quality. A study of the salinity of borehole water in the Ain El Atti region using hydrochemical methods revealed that the Ain El Atti site is characterized by a very saline infra-Cenomanian aquifer with high conductivities (ranging from 11 to 14.5 mS/cm) and chloride concentrations (ranging from 2800 mg/l to 4200 mg/l) [53]. The following Table1 gives the detailed composition of the borehole water (the water point N°4037/57) at the inlet of the reverse osmosis.

Table 1: The borehole water Ain El Atti analysis.

ECH	P13
Name	Ain El Atti (4037/57)
pH	6.5
Temperature (˚C)	24.1
Redox potential (mV)	0.30
Ion	Raw water (mg/l)
Hardness, as CaCO3	4206.79
Ca	1186.34
Mg	302.79
Na	807.71
K	132.86
Ba	0.032
Al	0.23
Ni	0.022
Pb	0.092
CO_3	0.44
HCO_3	900
SO_4	1449.20
Cl	3124.20
NO_3	0.10
CO_2	324.89
TDS	7904.02

3.1.2 Conversion rate (Y):

One of the most important elements in the design and sizing of a reverse osmosis unit is the conversion rate. As a result, selecting an optimum conversion rate should strike a balance between technical and economic issues [54]. The conversion rate (%Y) is defined as the ratio of the permeate flow rate to the feed rate using Eq. (1) [55]:

$$Y = 100\% \times (Q_p \,/\, Q_f) \qquad (1)$$

Where Q_p and Q_f are the permeate flow (m^3/h) and membrane supply water flow (m^3/h) values, respectively. We highlighted the following points in a comparison study conducted by Morocco's National Office of Drinking Water (ONEP) comparing the various conversion rates [56]:

- The energy consumption of the pumping units (at the level of the high-pressure unit) decreases with the increase of the conversion rate.
- The investment cost increases with the reduction of the conversion rate.
- The value of the conversion rate is limited by the solubility of the ions in the concentrate.
- The overall load of chemical reagents increases as the conversion rate decreases.

We chose a conversion rate of 75% to lower both the investment and the energy consumption of the RO unit. The production water flow will be 48.60 m^3/h since the input (feed) rate is 64.80 m^3/h (see Tab.2).

Table 2: The basic parameters of the RO unit.

Production flow (Q_p) at 24.1°C	48.60 m^3/h (1166.4 m^3/d)
Conversion rate (Y)	75%
Feed flow (Q_f)	64.80 m^3/h
Concentrate flow (Q_c)	16.20 m^3/h

3.2 Optimization of Ain El Atti borehole water RO unit:

The purpose of the Ain el Atti RO unit optimization was to compare the output of detailed reports of IMSDesign computer software employing dissimilar membrane products developed by Hydranautics. Thus, membrane selection was a significant property for the Ain el Atti RO unit optimization.

In reverse osmosis, the most used modules are spiral modules because this type of module is simpler, more efficient, and less expensive and requires low energy consumption [57, 58]. Spiral reverse osmosis modules are commercially available from several suppliers. However, more than 90% of the borehole water desalination sector is currently supplied by Hydranautics and Dow-Filmtec.

In this study, a pilot-scale cross-flow RO filtering system was employed. The pilot system is divided into two parts. The flow in a desalination RO membrane system is depicted (see Fig.2). A pump delivered the feed solution from the feed tank to the first stage, and the concentrate from the first stage was transported to the second step.

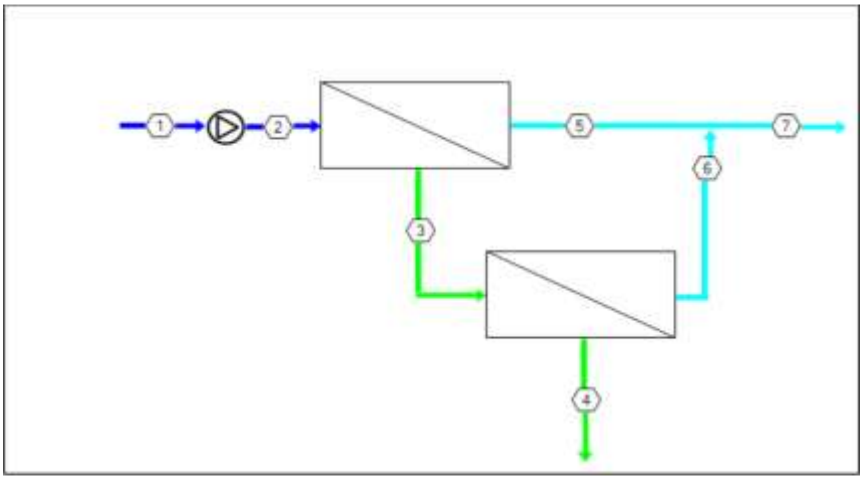

Figure 2: RO system schematic diagram.

Five different membrane modules provided by Hydranautics, using the Integrated Membrane Solutions (IMS) Design software were studied in the current work. Tab.3 shows a list of 8-inch (200 mm) diameter of the brackish manufacturer's membranes specifications [59, 60].

Table 3: Features of Hydranautics spiral-wound RO membrane elements.

Part Number	Size(mm) Diam.*Length	Surface Area (m^2)	Test Conditions (bar)	Permeate Flow (m^3/d)	Stabilized Rejection (%)
CPA3	200*1016	37.2	15.5	41.6	99.70
CPA5-LD	200*1016	37.2	15.5	41.6	99.70
CPA6-LD	200*1016	37.2	15.5	30.3	99.75
CPA7-LD	200*1016	37.2	15.5	43.5	99.80
ESPA2-LD	200*1016	37.2	10.3	37.9	99.60

For the choice of membranes used for this project, we have established a comparative study between the membrane's modules mentioned previously, using the IMSDesign software, version 2015 (from Hydranautics). The current section is broken down into two parts:

- The number of modules required to obtain the desired flow rate (48.60 m^3/h) is compared. On this basis, we attempted to reduce the number of modules required in order to save money on the investment. We discovered at the conclusion of this section that the supplier provides modules with a maximum active area of 37.2 m^2, allowing us to obtain a minimum number of modules.

- The second part consists of an energy comparison between the preselected membrane modules to choose the membrane that consumes the least energy for the same configuration.

The final results of the calculations performed according to each membrane element used are shown in Tab.4.

Table 4: Comparison of final results between Hydranautics membranes utilizing IMSDesign program.

Case No.	1	2	3	4	5	6
Element Type	CPA3	CPA5-LD	CPA6-LD	CPA7-LD	ESPA2-LD	CPA7-LD + ESPA2-LD
Recovery (%)	75	75	75	75	75	75
Pressure Vessels Configuration	2 stages	2 stages	2 stages	2 stages	2 stages	2 stages
No. PVs (1st and 2nd) stages	5-3	5-3	5-3	5-3	5-3	5-3
No. of Elements	48	48	48	48	48	48
No. of membranes per PVs	6	6	6	6	6	6
Nominal diameter, mm (8”)	200	200	200	200	200	200
Total Active Area (m^2)	37.20	37.20	37.20	37.20	37.20	37.20
Average Osmotic Pressure (bar)	4.60	4.60	4.60	4.60	4.60	4.60
Feed TDS (mg/l)	7904.02	7904.02	7904.02	7904.02	7904.02	7904.02
Feed Temperature (°C)	24.10	24.10	24.10	24.10	24.10	24.10
Average NDP (bar)	13.20	13.30	16.90	12.90	11.90	12.00
Feed Pressure (bar)	22.30	22.40	26.10	22.00	21.20	21.10
Feed Flow (m^3/h)	64.80	64.80	64.80	64.80	64.80	64.80
Permeate Flow (m^3/h)	48.60	48.60	48.60	48.60	48.60	48.60
Permeate TDS (mg/l)	149.79	135.02	89.24	110.63	229.13	188.49
Specific Energy (kWh/m^3)	1.03	1.03	1.20	1.01	0.98	0.97
Power (kW)	50.06	50.06	58.32	49.07	47.63	47.14
Average Flux (lmh)	27.20	27.20	27.20	27.20	27.20	27.20

According to IMSDesign program reports, the total dissolved solids (TDS) were 149.79 mg/l and the specific energy consumption was 1.03 kWh/m^3, while the feed pressure was 22.30 bar, as shown in Fig.3-(a). The element type CPA5-LD which delivers the same 99.7% nominal NaCl rejection as CPA3 elements but at 10% higher pressures. Moreover, Fig.3-(b) shows the results of installing the CPA5-LD membranes where the total soluble salts decreased to 135.02 mg/l at feed pressure 22.40 bar and the specific energy consumption remains stable to1.03 kWh/m^3. When CPA6-LD membrane was used, the dissolved salts decreased to 89.24 mg/l. However, the specific energy consumption increased to1.20 kWh/m^3 and the feed pressure was augmented to 26.10 bar see Fig.3-(c). The product TDS produced by installing CPA7-LD membranes is 110.63 mg/l, with a feed water pressure of 22.00 bar and an energy consumption rate of 1.01 kWh/m^3 (see Fig.3- (d)). There are no design warnings of installing this membrane type under these conditions. Fig.3-(e) presents the use of ESPA2-LD membranes, where water salinity produced is 229.13 mg/l which is higher than the salinity obtained by CPA3, CPA5- LD, CPA6-LD and CPA7-LD membranes. However, there is a slightly smallest pressure. The reason which makes this membrane disadvantage than the earlier that ESPA2-LD projected for the RO unit with higher TDS. From Fig.3-(f) it can be seen that the permeate TDS 188.49 mg/l is low compared with that of ESPA2-LD (229.13 mg/l). Furthermore, the feed pressure 21.10 bar is lower than the membranes existing feed pressure. Thus, the specific energy consumption 0.97 kWh/m^3 is smaller than the found membranes current specific energy consumption and without any design warnings suggested.

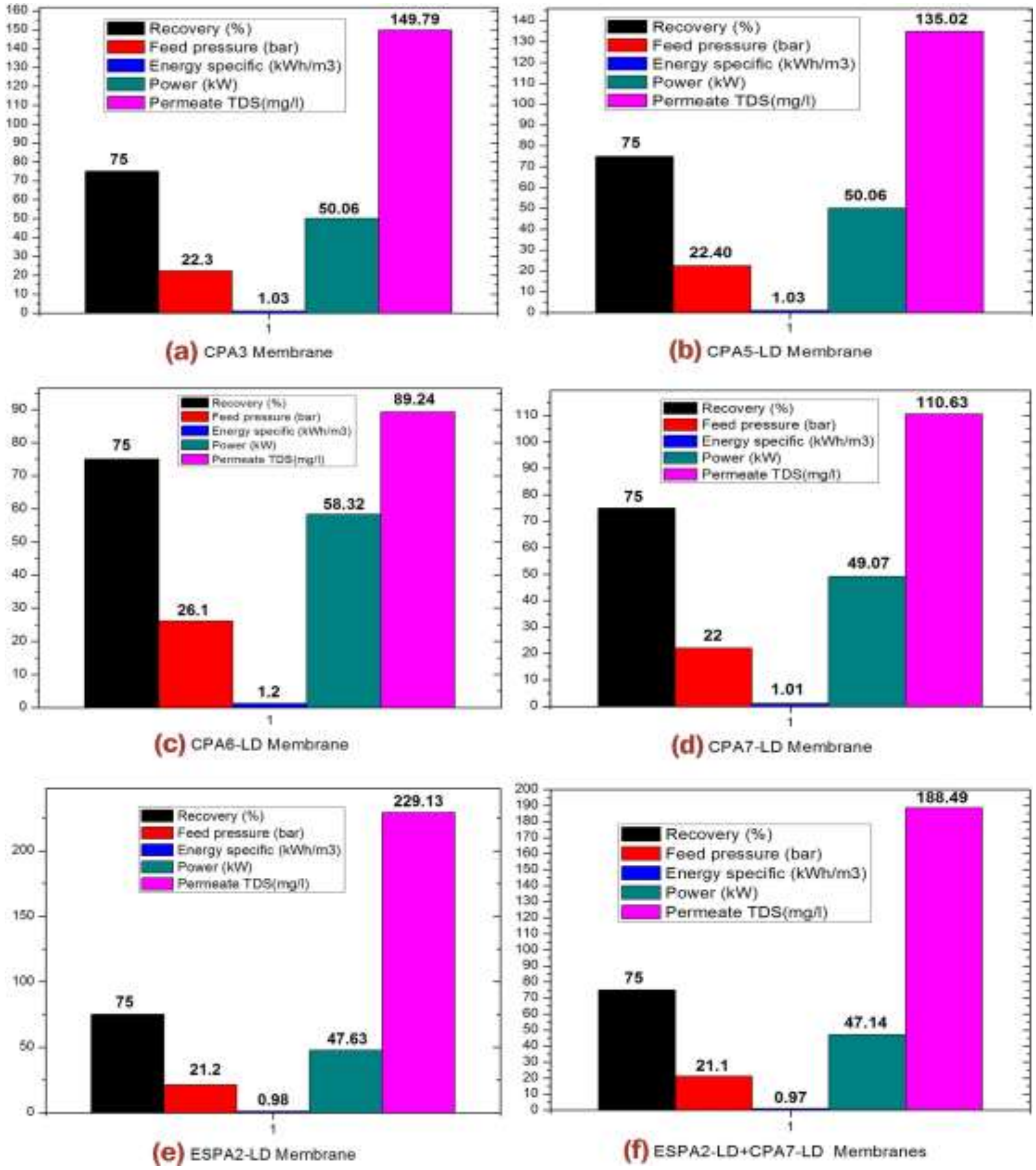

Figure 3: The results of using (a): CPA3, (b): CPA5-LD, (c): CPA6-LD, (d): CPA7-LD, (e): ESPA2-LD and (f): CPA7-LD+ESPA2-LD membranes for RO system.

Based on the previous design findings, it is possible to deduce that the CPA7-LD membrane is recommended for the first stage to achieve a high salt rejection rate and the ESPA2-LD membrane for the second stage to reduce energy consumption. RO system will be divided into two stages, with the first stage concentrate feeding the supply of the second stage on the one hand and a high-pressure group on the other. A second rescue high-pressure group, connected to reverse osmosis, will be provided to replace the main high-pressure group and ensure high pressure pumping under conditions comparable to the main group. Tab.5 summarizes the key findings of the reverse osmosis unit sizing.

Table 5: Results of the sizing of the RO unit.

Number of stages	Production capacity per stage (m^3/h)	Osmotic pressure (bars)	Membrane reference	Number of modules per stage	Number of Modules per pressure vessel	Number of pressure vessel
Stage 1	38.90	5.2	CPA7-LD	30	6	5
Stage 2	9.69	12.8	ESPA2-LD	18	6	3

3.3 Simulation of the performance of the system chosen by the IMSDesign program:

The IMSDesign software, allows us to check the performance of our reverse osmosis system, as well as the quality of reverse osmosis water, by introducing the following parameters:

- Quality of raw water.
- Feed flow rate.
- Design parameter (Temperature, pH, conversion rate).
- System configuration: number of stages, number of pressure vessels, number of modules per pressure vessel and membrane reference.

Fig.4 presents the detailed report results of the IMSDesign simulation. The results show that RO is extremely efficient because it decreases the ion concentrations in raw water. An examination of the obtained permeate in Fig.4 reveals that, with the exception of carbon dioxide (CO2), the ion concentrations meet World Health Organization (WHO) [61] and Moroccan criteria for drinking water meant for human consumption (NM 03-7-001) [62].

Project name	Ain El Atti		Page : 1/4
Calculated by	A.MAFTOUH	Permeate flow/train	48,60 m3/h
HP Pump flow	64,80 m3/h	Raw water flow/train	64,80 m3/h
Feed pressure	21,1 bar	Permeate recovery	75,00 %
Feed temperature	24,1 °C(75,4°F)	Element age	3,0 years
Feed water pH	6,50	Flux decline %, per year	5,0
Chem dose, mg/l, -	None	Fouling factor	0,86
Specific energy	0,97 kwh/m3	SP increase, per year	7,0 %
Pass NDP	12,0 bar	Inter-stage pipe loss	0,207 bar
Average flux rate	27,2 lmh		
		Feed type	Brackish Well Non-Fouling

Pass - Stage	Perm. Flow m3/h	Flow / Vessel Feed m3/h	Flow / Vessel Conc m3/h	Flux lmh	DP bar	Flux Max lmh	Beta	Stagewise Pressure Perm. bar	Stagewise Pressure Boost bar	Stagewise Pressure Conc bar	Perm. TDS mg/l	Element Type	Element Quantity	PV# x Elem #
1-1	38,9	13	5,2	35	1	44,3	1,16	0	0	20,1	60,2	CPA7-LD	30	5 x 6M
1-2	9,6	8,6	5,4	14,4	0,7	26	1,11	0	0	19,2	709,8	ESPA2-LD	18	3 x 6M

Ion (mg/l)	Raw Water	Feed Water	Permeate Water	Concentrate 1	Concentrate 2
Hardness, as CaCO3	4206,79	4206,79	45,806	16642,4	16642,4
Ca	1186,34	1186,34	12,918	2965,9	4693,3
Mg	302,79	302,79	3,297	757,0	1197,9
Na	807,71	807,71	41,482	2004,0	3097,9
K	132,86	132,86	8,482	328,9	504,6
NH4	0,00	0,00	0,000	0,0	0,0
Ba	0,032	0,032	0,000	0,1	0,1
Sr	0,000	0,000	0,000	0,0	0,0
Al	0,230	0,230	0,001	0,6	0,9
Ni	0,022	0,022	0,000	0,1	0,1
Pb	0,092	0,092	0,001	0,2	0,4
H	0,00	0,00	0,006	0,0	0,0
CO3	0,44	0,44	0,000	3,6	9,8
HCO3	900,00	900,00	39,796	2226,3	3444,7
SO4	1449,20	1449,20	8,631	3626,3	5754,3
Cl	3124,20	3124,20	73,862	7791,9	12239,3
F	0,00	0,00	0,000	0,0	0,0
NO3	0,10	0,10	0,015	0,2	0,4
PO4	0,00	0,00	0,000	0,0	0,0
OH	0,00	0,00	0,000	0,0	0,0
SiO2	0,00	0,00	0,000	0,0	0,0
B	0,00	0,00	0,000	0,0	0,0
CO2	342,89	342,89	342,89	342,89	342,89
TDS	**7904,02**	**7904,02**	**188,49**	**19704,95**	**30943,59**
pH	**6,50**	**6,50**	**5,25**	**6,85**	**7,02**

Saturations	**Raw Water**	**Feed Water**	**Concentrate**	**Limits**
CaSO4 / ksp * 100, %	88	88	497	400
SrSO4 / ksp * 100, %	0	0	0	1200
BaSO4 / ksp * 100, %	215	215	1040	10000
SiO2 saturation, %	0	0	0	140
CaF2 / ksp * 100, %	0	0	0	50000
Ca3(PO4)2 saturation index	0,0	0,0	0,0	2,4
CCPP, mg/l	407,94	407,94	2067,01	
Langelier saturation index	0,83	0,83	2,47	2,5
Ionic strength	0,19	0,19	0,73	
Osmotic pressure, bar	4,6	4,6	17,8	

Figure 4: Ain El Atti borehole water quality interface in IMSDesign-2015 software.

The problems related to dissolving CO2 in water to obtain practically neutral water can be avoided by increasing the pH to around 8.5 by adding caustic soda (also known as sodium hydroxide (NaOH)).

Table 6: Permeate characteristics based on the pH of the RO unit's feed water.

Increase method	Osmosis inlet pH	Permeate pH	CO_2 (mg/l) in the permeate
Without an increase of pH	6.5	5.25	342.89
Dosage of 349.7 mg/l NaOH	8.5	7.26	4.97

From the previous Tab.6, we note that increasing the pH to 8.5 with NaOH gives a lower concentration of CO_2 of 4.97 mg/l instead of 342.89 mg/l at pH=6.5. Using the IMSDesign software, we performed a simulation at a pH higher than 6.5 (pH=8.5) while keeping the same number of modules. The water quality results of this simulation are presented in Fig.5.

Ion (mg/l)	Raw Water	Feed Water	Permeate Water	Concentrate 1	Concentrate 2
Hardness, as CaCO3	4206,79	4206,79	44,813	16646,7	16646,7
Ca	1186,34	1186,34	12,638	3081,7	4694,5
Mg	302,79	302,79	3,226	786,5	1198,2
Na	807,71	1008,78	50,720	2601,0	3872,8
K	132,86	132,86	8,306	341,8	505,2
NH4	0,00	0,00	0,000	0,0	0,0
Ba	0,032	0,032	0,000	0,1	0,1
Sr	0,000	0,000	0,000	0,0	0,0
Al	0,230	0,230	0,001	0,6	0,9
Ni	0,022	0,022	0,000	0,1	0,1
Pb	0,092	0,092	0,001	0,2	0,4
H	0,00	0,00	0,000	0,0	0,0
CO3	0,44	63,97	0,063	483,5	1063,5
HCO3	900,00	1303,90	58,871	3080,7	4285,9
SO4	1449,20	1449,20	8,815	3767,7	5754,1
Cl	3124,20	3124,20	75,429	8094,9	12235,1
F	0,00	0,00	0,000	0,0	0,0
NO3	0,10	0,10	0,016	0,3	0,4
PO4	0,00	0,00	0,000	0,0	0,0
OH	0,00	0,05	0,003	0,1	0,1
SiO2	0,00	0,00	0,000	0,0	0,0
B	0,00	0,00	0,000	0,0	0,0
CO2	342,89	4,97	4,97	4,97	4,97
TDS	**7904,02**	**8572,51**	**218,09**	**22239,14**	**33611,14**
pH	**6,50**	**8,50**	**7,26**	**8,83**	**8,95**

Figure 5: Ain El Atti borehole water quality interface in the IMSDesign software at pH=8.5.

This change in pH increased the cost of reagents (the dose of NaOH at pH=8.5 is 349.7 mg/l versus no dose of NaOH at pH=6.5), as well as the supply pressure and, as a result, energy consumption (1.04 kWh/m^3 for the case of adding NaOH versus 0.97 kWh/m^3 for the case of not increasing the pH), as shown in Fig.6.

Project name	Ain El Atti		Page
Calculated by	A.MAFTOUH	Permeate flow/train	48,60 m3/h
HP Pump flow	64,80 m3/h	Raw water flow/train	64,80 m3/h
Feed pressure	22,5 bar	Permeate recovery	75,00 %
Feed temperature	24,1 °C(75,4°F)	Element age	3,0 years
Feed water pH	8,50	Flux decline %, per year	5,0
Chem dose, mg/l, 100 %	349,7 NaOH	Fouling factor	0,86
Specific energy	1,04 kwh/m3	SP increase, per year	7,0 %
Pass NDP	12,6 bar	Inter-stage pipe loss	0,207 bar
Average flux rate	27,2 lmh		

Figure 6: The value of the feed pressure and the specific energy when adding NaOH by using IMS- Design software.

3.4 Energy consumption:

The electricity consumption of a RO unit is a key criterion in determining the project's profitability since the high-pressure pump consumes over 80% of the energy required to operate a demineralization station for borehole water [63]. As a result, if reverse osmosis energy consumption is unchecked, the cost of drinking water can easily be multiplied.

Tab.7 summarizes the total energy requirement for the reverse osmosis demineralization plant for borehole water in the Ain El Atti zone.

Table 7: The energy demand of the reverse osmosis (RO) unit.

RO unit	Power (kW)
High-pressure pump (HPP)	67.39

This power will be raised by 5% to account for the demand for auxiliary electricity (lighting) and 10% to maintain a safety buffer. As a result, the station's total demand is 77.50 kW. This equates to an usage of 1.19 kWh/m^3. The plant's yearly production is anticipated to be 106 434 m^3/year while operating for 6 hours per day. As a result, the station consumes 126.66 MWh per year.

3.5. Sizing the components of PV generator:

3.5.1 PV module tilt angle:

The "Ain El Atti" research site is located in the Tafilalet plain, in the south-east of Morocco, on the southern slope of the High Atlas, at latitude 31.57°N, longitude 4.19°E, with an elevation of 854 m. PVsyst determines the best values (Fig.7) based on the previously determined site. The ideal tilt angle for yearly yield optimization is 34°, while the azimuth angle is 0° (south oriented).

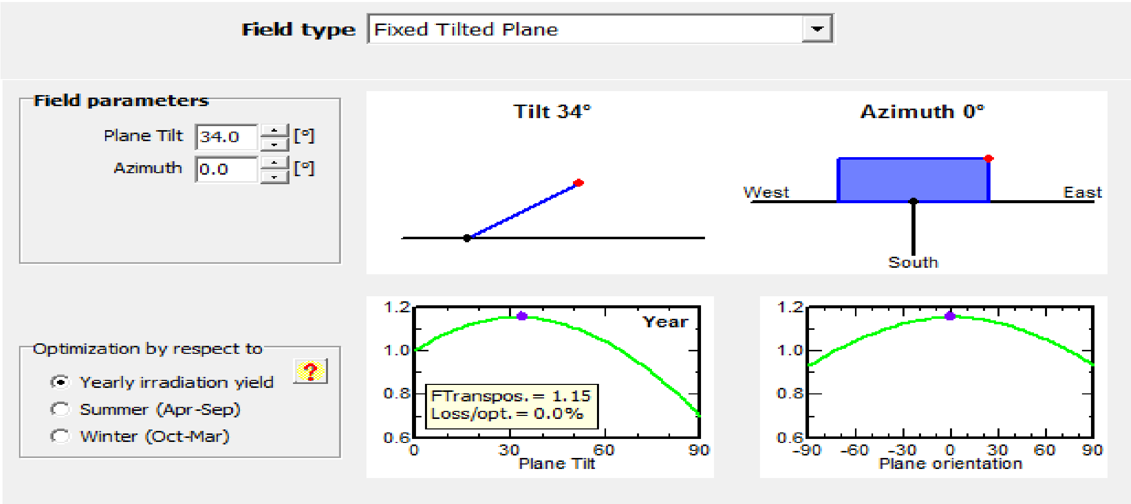

Figure 7: PVsyst screen shot of collector plane orientation.

The monthly average sun radiation at 34° tilt angle with zero azimuth angle was measured using local meteorological data from Ain El Atti, Errachidia (see Fig.8).

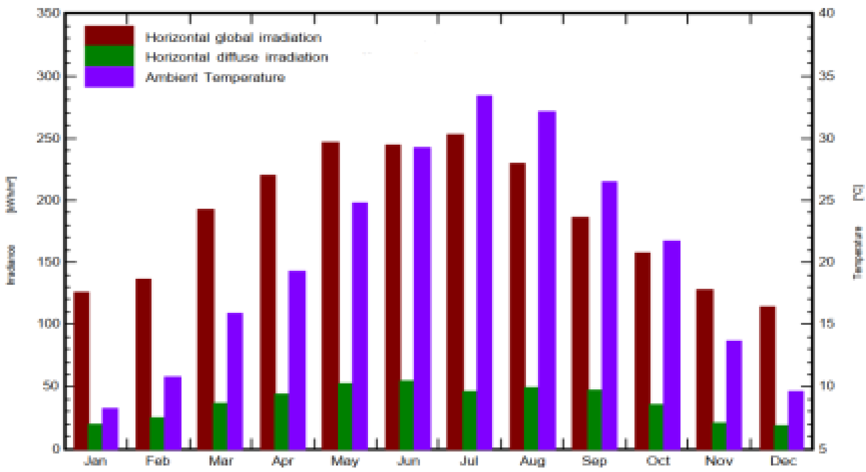

Figure 8: Different monthly variation of monthly solar irradiance data (kWh/m^2) at 34º tilt angle in Ain El Atti, Errachidia, and corresponding temperatures (ºC).

Ain El Atti gets 2232.7 kWh/m^2 of total incident global horizontal radiation every year, with an average Ambient Temperature (T_Amb) of roughly 20.47°C, or an annual average radiation of approximately 186.06 kWh/m^2 per month. Ain El Atti has the highest sun insolation in July. At 33.37°C, it is 252.7 kWh/m^2, which equates to 8.15 kWh/m^2/day. The month of December has the lowest solar irradiation (113.8 kWh/m^2 at 9.59°C, which is comparable to 3.67 kWh/m^2/day). This is caused by variations in the position of the sun in relation to the region in question.

After a simulation at a tilt angle of 34°, the incident radiation data on an inclined plane is obtained. As a result of adding the seasonal optimum tilt (34°) to the global horizontal radiation (GlobHor), the yearly total outcome (GlobInc) climbs to 2558.7 kWh/m^2. After lAM adjustment, effective radiation (GlobEff) data yields a result of 2513.3 kWh/m^2/year (see Fig.9).

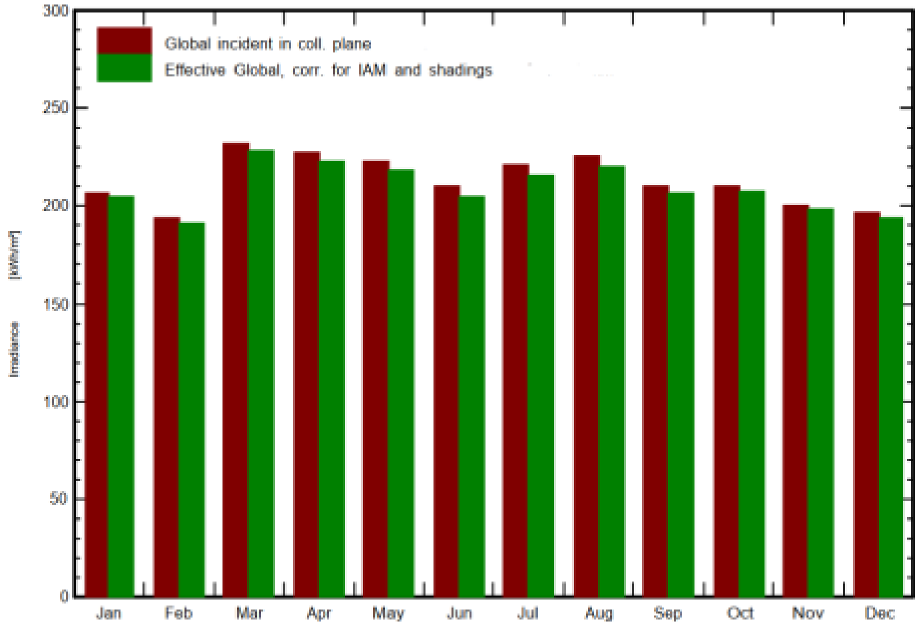

Figure 9: Global incident in coll. plane (GlobInc) and Effective Global, corrected for IAM and shadings (GlobEff) after all efficiency corrections have been applied.

3.5.2 Peak-PV power requirements:

The preceding subsection indicates that the energy requirements of the RO unit will be 347.004 kWh/day, however the inverter and thermal losses of the PV generator must be considered. Using Eq.(2) to calculate the PV temperature coefficient [64], and assuming that the PV modules will be 30°C higher than the ambient temperature (for winter months, December has the lowest solar radiation), the module temperature will be 39.59°C; for summer months (March has the lowest solar radiation), the module temperature will be 45.89°C, resulting in thermal losses in the PV system.

$$T_c = 1 - 0.005 \times (T_m - 20) \qquad (2)$$

The temperature correction factor (T_c) was calculated to be 0.902 for December and 0.870 for March, respectively. Assuming the inverter losses (L_{inv}) to be about 10% and the atmospheric dirt losses (L_{atmd}) about 10% for all months. The average peak sunshine hours (APSH) in Ain El Atti, APSH is 6 hrs. The peak PV array power (P_a) can be calculated from Eq. (3) as follows [65]:

$$P_a = E/(APSH \times T_c \times L_{inv} \times L_{atmd}) \qquad (3)$$

According to Eq. (3), the highest PV array power in December and March was 79.16 kW and 82.07 kW, respectively. As a result of these findings, the greatest value of peak power is chosen, and the required peak power is 82.07 kWp. As a result, the solar array must be large enough to produce 82.07 kWp.

3.5.3 PV arrays and Inverters:

The selection of PV arrays and inverters is a critical factor in the construction of an 82.07 kWp PV power plant. It is chosen such that the total number of PV panels and inverters utilized in the system's design is kept to a minimum, and the system's manufacturer. Tab.8 lists the selected modules and inverters, as well as their essential technical characteristics for the PV installation design. These two module technologies and inverters were chosen because they are now among the most extensively utilized in small-scale PV systems. For further details, see the technical datasheet [66–69].

Table 8: Specifications of different PV module technologies and Inverters used.

Technical Specifications of PV modules and Inverters		
Technology kind	Polycrystalline Silicon	CdTe Thin-Film
Manufacturer	Canadian Solar	First Solar
Model	CS6U–320P–AG	FS–4110–3
Cell Efficiency (%)	18.25	16.27
Module Efficiency (%)	16.46	15.28
Maximum PowerPoint (Wp)	320	110
Voltage in the Open Circuit (Voc); (V)	45.30	86.40
Isc (Short Circuit Current); (A)	9.26	1.82
Vmp (Maximum Power Voltage); (V)	36.80	67.80
Power Current Maximum (Imp); (A)	8.69	1.62
Type of Inverter	Central Inverter	Central Inverter
Manufacturer	Sungrow	SMA
Model	SG20KTL	Sunny Tripower 25000TL–30
Max. Efficiency (%)	98.00	98.30
Max. European Efficiency (%)	97.30	98.10
PV Input Voltage Maximum(V)	1000	1000
PV Input Current Maximum (A)	42.00	66.00
AC Output Power Nominal (kW)	20.00	25.00
Nominal Alternating Current Voltage (V)	400	400
AC Output Current Maximum (A)	33.00	36.20

3.5.4 PVsyst simulation yielded the following results:

PVsyst calculated four alternative scenarios, each with two different inverters and two different PV modules (see Tab.9). The PVsyst findings for the four scenarios are discussed, studied, and compared to determine which is the most advantageous module-inverter scenario with the best design outcomes.

Table 9: Selection of the PV module and the inverter for each of the four scenarios.

	PV module	Inverter
Scenario 1	Canadian Solar CS6U–320P–AG	Sungrow SG20KTL
Scenario 2	First Solar FS–4110–3	Sungrow SG20KTL
Scenario 3	Canadian Solar CS6U–320P–AG	SMA Sunny Tripower 25000TL–30
Scenario 4	First Solar FS–4110–3	SMA Sunny Tripower 25000TL–30

Tab.10 displays the findings obtained for the number of elements in the system as well as the installed capacity for each of the scenarios examined.

Table 10: The PVsyst findings for the four scenarios

	Scenario 1	Scenario 2	Scenario 3	Scenario 4
No. of PV modules in series	18	10	19	9
No. of PV modules in parallel	15	75	14	83
No. of Inverters	4	4	3	3
No. of PV modules	270	750	266	747
Installed capacity (kWp)	86.4	82.5	85.1	82.2

Table 10 shows that the number of modules in series in scenario 1 is more than the amount in scenario 2, despite the fact that both scenarios use the same inverter technology. This discrepancy is due to the MPP voltage and maximum open-circuit voltage of the modules being larger in scenario 2 than in scenario 1.

Fewer modules in series can be linked per inverter for larger module voltage levels. The same is true for situations 3 and 4, except that the PV modules chosen for scenario 3 have a lower MPP voltage and a lower minimum open-circuit voltage. When comparing Scenarios 1 and 3, which both employ the identical PV modules but different inverters, the number of PV modules in series in Scenarios 1 is fewer since the voltage values of the inverter used in Scenarios 3 are greater.

Scenarios with lower current levels for PV modules (Scenarios 2 and 4) enable for more PV modules to be connected in parallel per inverter. Scenario 4 enables for more PV modules to be connected in parallel than scenario 2 due to the use of an inverter with larger current input specifications (see Tab.10). Furthermore, the number of inverters in a solar system is proportional to the maximum permissible input power of the inverters. In contrast to scenarios 1 and 2, scenarios 3 and 4 employ a kind of inverter with a greater permitted input power, resulting in fewer inverters required in the PV solar power plant.

In Tab.10, we conclude that the value of the number of PV modules relies on both the kind of inverter used and, to a considerable degree, the PV module technology. The original design capacity of 82.07 kWp PV plant is changed differently for all scenarios according to the amount of modules in series, modules in parallel, and inverters found in Tab.10; all scenarios are somewhat larger. Scenario 4 is the closest to design capacity, with an estimated installed capacity that is 0.15 % larger than the initial design capacity of 82.07 kWp. Scenario 1 has the greatest change, with an installed capacity that is 5.27 % more than the baseline number.

Tab.11 depicts the numbers obtained using PVsyst for the computations of the area occupied by the PV system for the four scenarios. It can be seen that the surface area of the PV system is relatively comparable in all cases, and it is roughly 530 m^2. As a result, the variance in the values obtained is driven by variations in the actual output power of the various situations.

Table 11: PVsyst values for the area occupied by the PV system.

	Scenario 1	Scenario 2	Scenario 3	Scenario 4
Area occupied by PV system (m^2)	530	540	522	538

The figures obtained in the PVsyst simulations for annual energy production (AEP) and specific yield ($Yield_{sp}$) for the four scenarios are shown in Tab.12. Furthermore, the findings for total yearly energy provided to the grid are derived from the output power of the DC/AC inverters and the application of losses due to the connecting transformer and the AC side cable. As a result, scenario 2 has the greatest value of roughly 183.3 MWh/year, followed by scenarios 4 and 1, which have values of 182.4 MWh/year and 182.1 MWh/year, respectively. Finally, scenario 3 has the lowest value, with a value of 179.2 MWh/year.

Table 12: Values for AEP and $Yield_{sp}$ by the PV systems for each of the studied scenarios.

	Scenario 1	Scenario 2	Scenario 3	Scenario 4
AEP (MWh/year)	182.1	183.3	179.2	182.4
$Yield_{sp}$ (kWh/kWp)	2108	2221	2105	2219

According to Tab.12, the yearly specific energy ($Yield_{sp}$), which is defined as the annual final energy output divided by the system's installed capacity, is 2108 kWh/kWp, 2221 kWh/kWp, 2105 kWh/kWp, and 2219 kWh/kWp for scenarios 1, 2, 3, and 4. Furthermore, specific energy may be utilized to evaluate the performance of PV systems put under similar climatic circumstances. As a result, based on energy production, the PV systems of scenarios 2 and 4 are the best possibilities, whereas scenarios 1 and 3 are the least acceptable solutions for the previously chosen location.

The performance ratio (PR), which depicts the influence of losses on the design power output of PV systems, is examined in this section. The performance ratio of the PV systems in the four examined situations is depicted in Fig.10. Furthermore, the performance ratio varies across different types of PV module and inverter technology. The yearly PR for scenarios 1, 2, 3, and 4 is 82.4 %, 86.8 %, 82.3 %, and 86.7 %, respectively. It can also be shown that the PRs of scenarios 2 and 4 have the greatest PRs, while the PRs of scenarios 1 and 3 have the lowest throughout the same location chosen for this study (see Fig.10). However, all possibilities have a probability of success greater than 80%. According to the International Finance Corporation (IFC), a well-designed PV system should have a performance ratio of between 77 and 87 % [70].

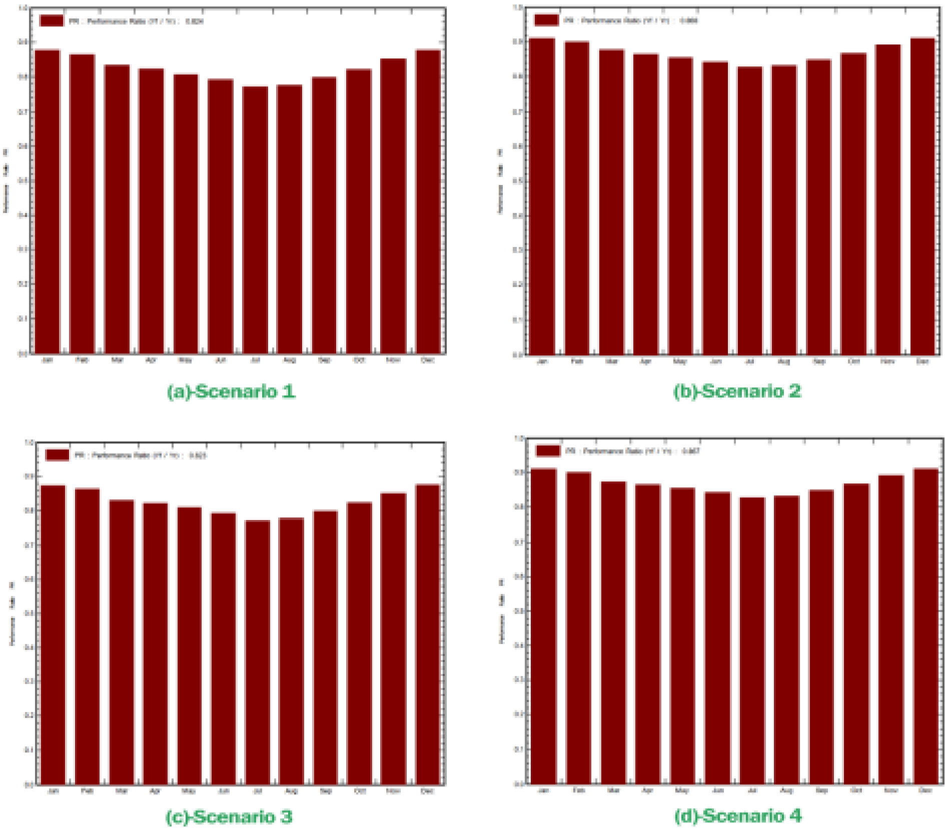

Figure 10: The annual performance ratio (PR) for the four scenarios

Fig.11 depicts the overall losses in the PVsyst-generated systems for all scenarios, as well as the energy generation after each simulation phase. These numbers do not give any more information, but they do highlight the contrasts between the four situations. The following are the findings reached:

• The beginning energy values for each scenario are derived using PV panels that have been functioning at Standard Test Conditions (STC) with no losses for a year. The variations in beginning values between scenarios are due to variances in installed capacity (see Tab.10).

• The biggest system losses are caused by the irradiance and temperature factors, as the PV modules do not always operate at STC. As a result, irradiance/temperature losses are the same in situations employing the same type of PV module.

• The losses of PV modules are the same in all situations that employ the same PV module technology. For scenarios 1 and 3, the ohmic wiring loss, module quality loss, and module mismatch loss are set as 1.34 %, 0.40 %, and 1.10 %, respectively. As a result, the total of these losses is 2.84 %. In contrast, the entire amount of PV module losses in scenarios 2 and 4 is 3.31 %.

• The losses due to inverter loss during operation (efficiency) are equal in scenarios 1 and 2, which share the same type of inverter Sungrow SG20KTL (losses of about 2.18 %), and the losses due to the efficiency of inverter SMA Sunny Tripower 25000TL–30 are 2.00 % and 2.14 %, respectively, in scenarios 3 and 4.

• For scenarios 1, 2, 3, and 4, the losses attributable to inverter loss over nominal inverter power are 0.05 %, 0.01 %, 0.36 %, and 0.13 %, respectively (see Fig.11- (a, b, c and d). These losses may be observed to change in various cases since they are affected by the output power of the solar panels and the parameters of the chosen inverter. The energy output of the DC/AC inverters refers to the energy output after applying the losses due to inverter performance.

• The efficiency of the process obtained using PVsyst is 16.68 % for scenario 1, 11.76 % for scenario 2, 16.81 % for scenario 3, and 11.85 % for scenario 4. As a consequence, scenarios 1 and 3 with the same module technology (pc-Si modules) have nearly the same efficiency, but scenarios 2 and 4 with CdTe modules have nearly the same efficiency.

In summary, scenarios utilizing poly-crystalline Silicon (pc-Si) PV modules provide less increased process efficiency than situations utilizing a thin-film CdTe module. In these computation scenarios, the changes in process efficiency owing to inverter technology are not substantial.

In conclusion, the calculation approach for a small-scale solar PV grid-connected energy system design is valid since the findings returned by the PVsyst simulation are consistent with those reported in the literature. In this sense, Scenario 2 is important since it shows the maximum annual energy production (AEP), performance ratio (PR), and specific yield ($Yield_{sp}$).

Figure 11: Losses diagram obtained with PVsyst for four scenarios.

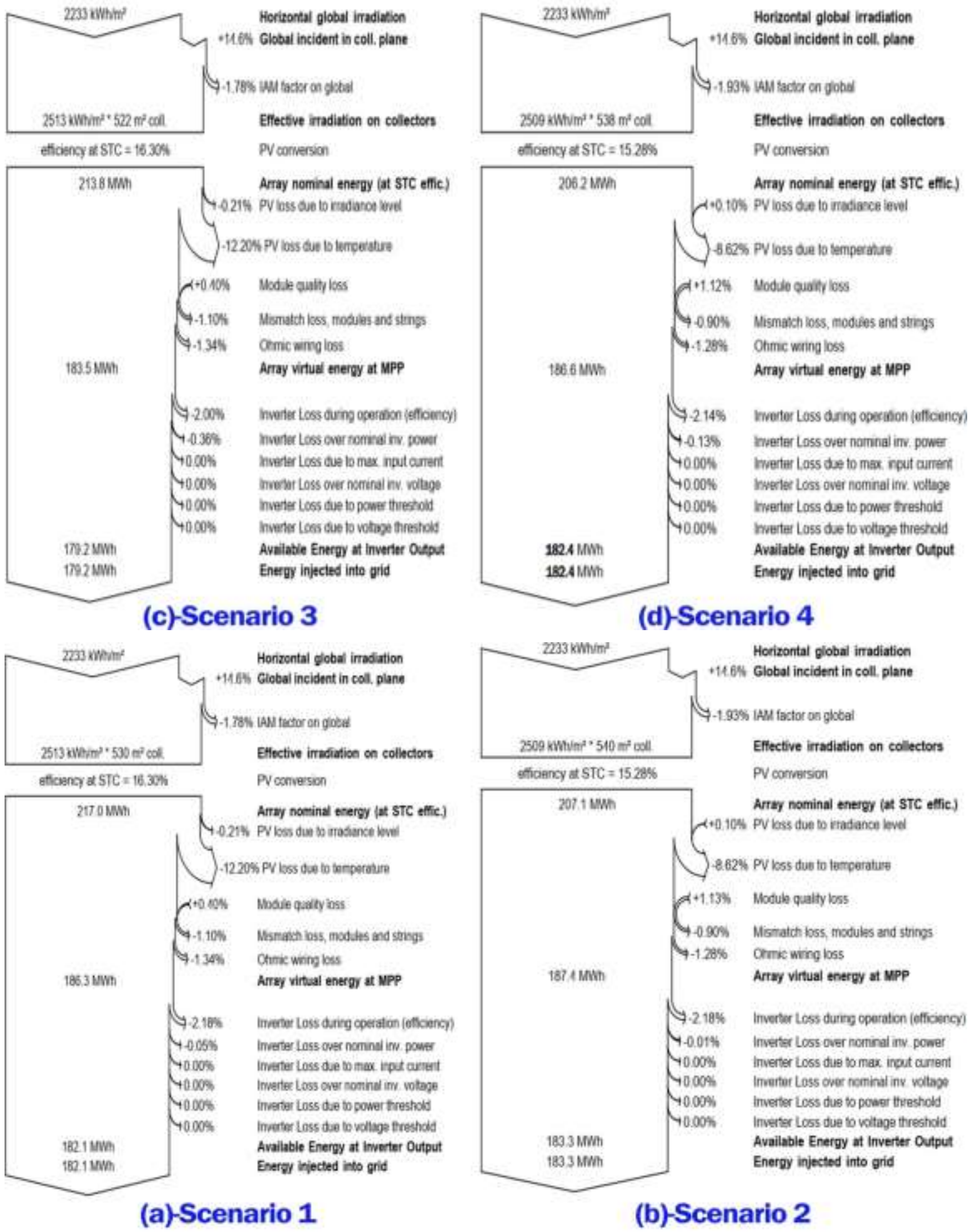

CONCLUSION:

In the face of rising freshwater demands, the Ain El Atti area is left with just one option: reverse osmosis water demineralization. This series of studies has demonstrated the energy, economic, and environmental benefits of using PV solar energy to power the Ain El Atti area's demineralization facility for borehole water. A significant contribution has been made to comparing the performances of RO membranes produced by the Hydranautics firm in order to create fresh water from Ain El Atti borehole water. It refers to highly important economic concerns concerning water quality in the examined region, as well as the optimization of energy usage in demineralization stations employing RO technology. The findings of the IMSDesign software's sizing simulation for the Ain El Atti borehole water reveal that the CPA7-LD membrane is recommended for the first stage to achieve a high salt rejection rate and the ESPA2-LD membrane for the second stage to decrease energy consumption. The results show that the water quality generated is satisfactory in accordance with Moroccan and WHO drinking water standards, however it has a slightly acidic pH and requires basic treatment to avoid corrosion. It demonstrates a high concentration of CO2 in water, necessitating the addition of NaOH to avoid difficulties caused by dissolved CO2 in generated water. Given the favorable national environment for renewable energy development, we conducted a sizing research of reverse osmosis (RO) unit and photovoltaic (PV) solar energy system coupling. In this case, the PVsyst software is used for data evaluation, sizing, and analysis for the intended small-scale solar PV grid-connected energy system, which combines two different module technologies and two different solar inverters to obtain the best possible configuration under the climatic conditions of the Ain El Atti region. The annual energy production (AEP) of four scenarios is used to calculate performance indicators such as the performance ratio (PR). The scenario with the greatest outcomes is one that employs CdTe thin-film module technology and inverters with the highest nominal power. The primary findings achieved for this scenario are 750 PV modules and 4 inverters; an installed capacity of 82.50 kWp; a PV module area of 540 m2; an AEP of 183.3 MWh/year; and evaluation metrics of 86.8 % PR and 2221 kWh/kWp $Yield_{sp}$. As a result, the findings obtained can surely be beneficial for determining the actual performance of a PV installation in real life, as well as providing important information about the optimal module-inverter combination, taking into consideration the conditions present at the Ain El Atti location.

REFERENCES

[1] B. Ammary, Geochemical and isotopic study of the main aquifers of the Cretaceous Basibn of Er-Rachidia and the Tafilalt plain. (2007) Thesis, Doc. Uni. Med V Agdal, Rabat, p. 134 (in French).

[2] L. Bouchaou et al., Origin and residence time of groundwater in the Tadla basin (Morocco) using multiple isotopic and geochemical tools, Journal of Hydrology, (2009) Vol. 379, pp. 323–338.

[3] M. Amharref, Contribution to the Hydrological study of the valley of the Ziz (province of Er-Rachidia in the south east of Morocco): the respective effects of drought and the Hassan Addakhil dam on the downstream water resources. Thesis, Uni. Besançon, (1991) p. 232 (in French).

[4] N. Warner et al., Integration of geochemical and isotopic tracers for elucidating water sources and salinization of shallow aquifers in the sub-Saharan Draa Basin, Morocco, Applied Geochemistry, (2013) Vol. 34, pp. 140–151.

[5] Directorate of Water Research and Planning (Direction de la Recherche et de la Planification de l'Eau (DRPE)), Establishment and development of groundwater management models for the Goulmima basin, Er-Rachidia.(1989), Internal report (in French).

[6] DRPE, Synthesis of hydrological data and work carried out in the Errachidia and Goulmima sedimentary basin. (1984), Internal report (in French).

[7] Y. M. Kim et al., Overview of systems engineering approaches for a large-scale seawater desalination plant with a reverse osmosis network, (2009) Desalination, Vol. 238, pp. 312–332.

[8] L. Malaeb et al., Reverse osmosis technology for water treatment: state of the art review, Desalination, (2011), Vol. 267, pp. 1–8.

[9] H. Strathman, Membrane Handbook, Van Nostrand Reinhold Electrodialysis, in: W.S.H.Ho, K.K. Sirkar (Eds.), (1992) New York, pp. 217–262.

[10] M. A. Sanz, Energy as motor of seawater reverse osmosis desalination development, Oral Presentation in Mega-ton Symposium New Energy and Industrial Technology Development Organization, (NEDO), Tokyo, (2013).

[11] M. Kurihara, Membrane research for water treatment facing the age of global mega competition & collaboration, Oral Presentation in Project Leader's Summit at IWA- ASPIRE 2011, Tokyo, (3 October, 2011).

[12] D & WR, 2006: Vol. 16, Issue 2, pp. 10–22.

[13] N. Carter, Desalination and membrane technologies: federal research and adoption issues, Congressional Research Service, (2015),Vol. 700, pp. 7–5.

[14] M. Moonkhum et al., Review of seawater natural organic matter fouling and re- verse osmosis transport modeling for seawater reverse osmosis desalination, Journal of Desalination and Water Treatment, (2010) Vol. 15, pp. 92–107.

[15] A. Zhu et al., Minimization of energy consumption for a two pass membrane desalination: effect of energy recovery, membrane rejection and retentate recycling, Journal of Membrane Science, (2009), Vol. 339, pp. 126–137.

[16] A. Zhu et al., Effect of stream mixing on RO energy cost minimization, Desalination, (2010) Vol. 261, pp. 232–239.

[17] A. Zhu et al., Reverse osmosis desalination with high permeability membranes - cost optimization and research needs, Desalination and Water Treatment, (2010), Vol. 15, pp. 256–266.

[18] A. Zhu et al., Effect of thermodynamic restriction on energy cost optimization of RO membrane water desalination, Industrial & Engineering Chemistry Research, (2009),Vol. 48, pp. 6010–6021.

[19] R. Karuppiah et al., Optimal design of reverse osmosis based water treatment systems, AIChE Journal, (2012), Vol. 58, pp. 2758–2769.

[20] F. Vince et al., Multi-objective optimization of RO desalination plants, Desalination, (2008), Vol. 222, pp. 96–118.

[21] Y.-y. Lu et al., Optimum design of reverse osmosis seawater desalination system considering membrane cleaning and replacing, Journal of Membrane Science, (2006), Vol. 282, pp. 7–13.

[22] S. Kamal et al., Effective design of reverse osmosis based desalination process considering wide range of salinity and seawater temperature, Desalination, (2012), Vol. 306, pp. 8–16.

[23] S. Kamal et al., MINLP based superstructure optimization for boron removal during desalination by reverse osmosis, Journal of Membrane Science, (2013), Vol. 440, pp. 29–39.

[24] A. Zhu et al., On RO membrane and energy costs and associated incentives for future enhancements of membrane permeability, Journal of Membrane Science, (2009), Vol. 344, pp. 1–5.

[25] A. Al-Karaghouli and L. L. Kazmerski, Energy consumption and water production cost of conventional and renewable-energy-powered desalination processes, Renewable and Sustainable Energy Reviews, (2013), Vol. 24, pp. 343–356.

[26] S. Vighetti, Photovoltaic systems connected to the network: Choice and dimensioning of the conversion stages. Thesis, Doc. Uni. Grenoble, (2010),n60052110 (in French).

[27] M. Nfaoui and K. El-Hami, Extracting the maximum energy from solar panels, Energy Reports, (2018), Vol. 4, pp. 536–545.

[28] M. El Ouariachi et al., Optimization and Modelling of Electrical Energies Produced by the Photovoltaic Panels and Systems, 18th Mediterranean Conference On Control and Automation, IEEE, ISBN 978-1-4244-8091-3/10/ IEEE, (2010), pp. 1614-1619.

[29] C. Charcosset, A review of membrane processes and renewable energies for desalination, Desalination, (2009) Vol. 245, pp. 214–231.

[30] A. Alkhatib, Reverse-Osmosis Desalination of Water Powered by Photo-Voltaic Modules, computational Water, Energy, and Environmental Engineering, (2014), Vol. 3, pp. 22– 29.

[31] M. G. Buonomenna and J. Bae, Membrane processes and renewable energies, Renewable & Sustainable Energy Reviews, (2015), Vol. 43, pp. 1343–1398.

[32] N. Ghaffour et al., Renewable energy-driven desalination technologies: A comprehensive review on challenges and potential applications of integrated systems. Desalination, (2015), Vol. 356, pp. 94–114.

[33] H. Sharon and K. S. Reddy, A review of solar energy driven desalination technologies, Renewable & Sustainable Energy Reviews, (2015), Vol. 41, pp. 1080–1118.

[34] M. S. Mohsen and O. R. AI-Jayyousi, Brackish water desalination: an alternative for water supply enhancement in Jordan, Desalination, (1999), Vol. 124, pp. 163–174.

[35] J. Rheinländer and F. Gräter, Technologies for the desalination of typically 10 m^3/d of water- DESAL10—a tool for the identification of appropriate de-central solutions, Desalination,(2001), Vol. 139, pp. 393–397.

[36] I. Houcine et al., Renewable energy sources for water desalting in Tunisia, Desalination, (1999), Vol. 125, pp. 123-132.

[37] D. Herold et al., Small scale photovoltaic RO desalination—Experiences in Gran Canaria. Proc. ISES Solar World Congress, Jerusalem, Israel, (6-13 July, 1999).

[38] International Renewable Energy Agency (IRENA), Water desalination using renewable energy, IEA-ETSAP and IRENA, (2012).

[39] L. Garcia-Rodrigues, Seawater desalination driven by renewable energies: A review, Desalination, (2002), Vol. 143, pp. 103–113.

[40] S. Lattemann et al., Global Desalination Situation, Sustainability Science and Engineering, (2010), Vol. 2, no. Sustainable water for the future.

[41] The World Bank, Renewable Energy Desalination - An Emerging Solution to Close the Water Gap in the Middle East and North Africa, The World Bank, Washington, D.C., (2012).

[42] K. Quteishat and Abu-Arabi, Promotion of Solar Desalination in the MENA Region, Middle East Desalination Research Center, Muscat, Oman, (2012).

[43] V. G. Gude, N. Nirmalakhandan, and S. Deng, Renewable and sustainable approaches for desalination, Renewable and Sustainable Energy Reviews, (2010), Vol. 9, pp. 2641–2654.

[44] Fraunhofer Institut for Solar Energy Systems ISE, Levelized Cost of Electricity Renewable Energy Technologies, Fraunhofer ISE, Freiburg, (2013).

[45] W. Khiari, M.Turki, and J. Belhadj, Power control strategy for PV/Wind reverse osmosis desalination without battery, Control Engineering Practice, (2019), Vol. 89, pp. 169–179.

[46] I. Ben Ali et al., Optimized fuzzy rule-based energy management for a battery-less PV/Wind-BWRO desalination system, Energy Journal, (2018), Vol. 159, pp. 216–228.

[47] B. S. Richards and A. I. Schafer, Renewable Energy Powered Water Treatment Systems, no. Sustainable Water for the Future: Water Recycling Versus Desalination, Sustainability Science and Engineering, (2010), Vol. 2, pp. 353–371.

[48] Z. Lgourna et al., Elucidating the sources and mechanisms of groundwater salinization in the Ziz Basin of southeastern Morocco, Environmental Earth Sciences, (2015), Vol. 73, pp. 77–93.

[49] Hydranautics, Integrated Membrane Solutions (IMS) Design Software version , (2015).

[50] K.P. Mehta and A.S. Patel, Treatment of waste water to meet disposal standards & to explore the possibilities for reuse of wastewater of common effluent treatment plant, water special volume, Environmental Pollution and Control, (2012), Vol. 15, pp. 67–70.

[51] [Online]. Available: http://photovoltaic-software.com/pvgis.php.

[52] A. Bruno and M. Wittmer, 2014: PVsyst User's Manual, [Online]. Available: https://www.pvsyst.com/images/pdf/PVsyst%20Tutorials.pdf.

[53] H. Dakkak et al., Contribution of the piezometric and hydrochemistry techniques to the characterization Ain El Atti groundwater table (Tafilalet), Proceedings of the International Symposium on the Sustainable Development of Oasian Systems from 8 to 10 March, (2005) Erfoud, Morocco–B. Boulanouar & C. Kradi (Eds.).

[54] P. Aimar, The fouling of the membranes. Advanced course « Membrane separation techniques » (Le fouling des membranes. Cycle de perfectionnement « Techniques de séparation sur membranes »), CERIA- Brussels, 1989 (in French).

[55] F. Elazhar et al., Economical evaluation of the fluoride removal by nanofiltration, Desalination, Vol. 249, (2009), pp. 154–157.

[56] Desalination of seawater and brackish water, Morocco's National Office of Drinking Water (ONEP) internal documents.

[57] G. Daufin, F. René, and P. Aimar, Membrane separations in food industry processes, Published by TEC ET DOC, France, (1998), p. 592.

[58] R. W. Baker, Reverse Osmosis in Membrane Technology and Applications, 2nd edition, John Wiley & Sons, Ltd.: Chichester, (2004), p. 191.

[59] CPA (Composite Polyamide) Membrane Technical Information, [Online]. Available: http://membranes.com/solutions/products/ro/cpa/.

[60] ESPA (Energy Saving Polyamide) Membrane Technical Information, [Online]. Available: http://membranes.com/solutions/products/ro/espa/.

[61] WHO, Guidelines or Drinking-Water Quality, 4th Edition, World Health Organization, Geneva, (2011).

[62] P. Roccaro et al., Water intended for human consumption—Part I: Compliance with European water quality standards, Desalination,(2005), Vol. 176, pp. 1–11.

[63] P. Corsin, Coll., Desalination of seawater by reverse osmosis: the real needs in energy, water, industry, pollution (Dessalement de l'eau de mer par osmose inverse : les vrais besoins en énergie, l'eau, l'industrie, les nuisances), N° 226, (2005), p. 5 (in French).

[64] K. Kangarakis, Photovoltaic Technology, Athens, 1992. (in Greek).

[65] G.-E. Ahmad, M.-A. Mohamd, Energy Conversion and Management, (2000), Vol. 41, Issue12, pp. 1293–1301.

[66] Canadian Solar, "MAX POWER 2 CS6U–315| 320| 325| 330P", [Online]. Available: https://www.solaris-shop.com/content/CS6U-330P 20Specs.pdf.

[67] First Solar, "First Solar Series 4 PV Module", [Online]. Available: http://www.firstsolar.com/en-EMEA/-/media/First-Solar/Technical-Documents/Series-4-Datasheets/Series-4V3-Module-Datasheet.ashx.

[68] Sungrow, "SG20KTL", [Online]. Available: https://www.pekat.com.my/pdf/Sungrow-SG20KTL.pdf.

[69] SMA, "Sunny Tripower 15000TL / 20000TL / 25000TL", [Online]. Available: https://files.sma.de/dl/24336/STP25000TL-30-DEN1742-V31web.pdf.

[70] IFC, International Finance Corporation, Utility-Scale Solar Photovoltaic Power Plants, Washington, D.C., (2015).